Engineering Research Express

INCLUSIVE PUBLISHING TRUSTED SCIENCE

PURPOSE-LED PUBLISHING™

**PAPER** • **OPEN ACCESS**

# Charge recombination suppression as the key factor governing DSSC performance: a comparative study of *Campsis radicans, Consolida orientalis*, and *Glaucium grandiflorum*

To cite this article: M Erdoğdu *et al* 2026 *Eng. Res. Express* **8** 215002

View the article online for updates and enhancements.

You may also like

- SARSegNet: deep learning segmentation network for land cover object segmentation from SAR images
Vishal Mukundan, Vibha Damodra Kevala, Sravya N et al.
- Multi-objective parametric optimization of chemical mechanical polishing for BK7 optical glass using RSM-NSWOA-TOPSIS
Xincheng Yin, Zikai Wang, Huijun Han et al.
- Lightweight band-guided hierarchical fusion network for defect segmentation of carbon fiber-reinforced composites in infrared thermograms
Qingyun Tang, Fengxia Han, Bin Liu et al.

This content was downloaded from IP address 95.183.211.218 on 15/11/2026 at 21:08

Engineering Research Express

Check for updates

OPEN ACCESS

RECEIVED
2 July 2026

REVISED
21 September 2026

ACCEPTED FOR PUBLICATION
16 October 2026

PUBLISHED
6 November 2026

Original content from this work may be used under the terms of the Creative Commons Attribution 4.0 licence.

Any further distribution of this work must maintain attribution to the author(s) and the title of the work, journal citation and DOI.

PAPER

# Charge recombination suppression as the key factor governing DSSC performance: a comparative study of *Campsis radicans*, *Consolida orientalis*, and *Glaucium grandiflorum*

**M Erdoğdu[1], K Ozel[2,3], M E Yelkovan[3,4], A Yildiz[3,5], B Altun[6] and Y Erdogdu[7,*]**

[1] Department of Landscape Architects, Faculty of Agriculture, Kırşehir Ahi Evran University, Kırşehir 40100, Türkiye
[2] Department of Electrical and Energy, GAMA Vocational School, Ankara University, 06120 Ankara, Türkiye
[3] The Center for Third Generation Solar Cells Research and Applications (SUN 3.0), Ankara Yıldırım Beyazıt University, 06170 Ankara, Türkiye
[4] AYBU Central Research Laboratory, Ankara Yildirim Beyazit University, 06010 Ankara, Türkiye
[5] Department of Energy Systems Engineering, Faculty of Engineering and Natural Sciences, Ankara Yildirim Beyazıt University, 06010 Ankara, Türkiye
[6] Department of Horticulture, Faculty of Agriculture, Kırşehir Ahi Evran University, Kırşehir 40100, Türkiye
[7] Department of Physics, Faculty of Science, Gazi University, 06500 Teknikokullar, Ankara, Türkiye
[*] Author to whom any correspondence should be addressed.

**E-mail:** merdogdu@ahievran.edu.tr, kenanozel89@gmail.com, meyelkovan@aybu.edu.tr, yildizab@gmail.com, bahadir.altun@ahievran.edu.tr and yerdogdu@gazi.edu.tr

**Keywords:** dye-sensitized solar cells, *Campsis radicans*, *Consolida orientalis*, *Glaucium grandiflorum*, photovoltaic performance, charge recombination

## Abstract

In the present work, three plant-derived natural dyes extracted from *Campsis radicans* (*CR*), *Consolida orientalis* (*CO*), and *Glaucium grandiflorum* (*GG*) were investigated as sensitizers for dye-sensitized solar cells (DSSCs). The Fourier-transform infrared spectra (400–4000 $cm^{-1}$ region) of the natural dyes verified the existence of functional groups that facilitate their adsorption onto $TiO_2$ surfaces. UV–vis spectra of the dye and the dye-loaded photoanodes indicated improved light absorption in the visible region (400–700 nm), with *CR* presenting the strongest absorption response. The *CR*-based DSSC presented the highest photovoltaic performance with a power conversion efficiency of 0.78%, an open-circuit voltage ($V_{OC}$) of 0.61 V, and a fill factor of 55%. Additionally, the electrochemical impedance spectroscopy analysis showed that the *CR*-based DSSC device exhibited better charge-collection behavior and recombination resistance than the other devices. The observed increase in recombination resistance indicates suppressed interfacial electron losses, which contribute to the enhanced photovoltaic performance. These results suggest that, alongside efficient light harvesting, suppression of charge recombination plays a crucial role in determining the efficiency of natural dye-sensitized DSSCs.

## 1. Introduction

Dye-sensitized solar cells (DSSCs) have attracted considerable attention as a photovoltaic technology owing to their low fabrication costs, straightforward manufacturing procedures, and potential for sustainable energy conversion. Unlike conventional silicon-based solar cells, DSSCs operate through a photoelectrochemical mechanism in which light harvesting, electron injection, and charge transport occur at distinct interfaces within the device architecture. Consequently, the sensitizer plays a central role in determining photovoltaic performance by governing both photon absorption and interfacial electron-transfer processes [1].

The highest power conversion efficiencies (PCEs) reported for DSSCs have generally been attained using ruthenium-based complexes and synthesized organic dyes. Nonetheless, the extensive use of these sensitizers is constrained by factors such as high production costs, multistep synthesis processes, and environmental concerns. The aforementioned limitations have prompted heightened interest in

© 2026 The Author(s). Published by IOP Publishing Ltd

alternative sensitizers sourced from renewable natural resources [2, 3]. Natural dyes from biological sources have attracted considerable interest due to their availability, biocompatibility, and eco-friendliness, as well as extraction methods. The use of renewable resources has been encouraged.

Natural dyes are a large family of photoactive materials, whose photoactivity is related to the presence of light-absorbing constituents such as anthocyanins, flavonoids, tannins, and other polyphenolics. The chemical structure of these molecules, in particular the presence of hydroxyl and carbonyl functional groups, enables efficient coupling to $TiO_2$ surfaces, resulting in stable dye adsorption and efficient injection of photoexcited electrons. Nevertheless, exploiting these beneficial properties to achieve competitive photovoltaic outputs remains challenging. Unlike synthetic alternatives, natural dyes are often limited by poorer surface binding, less efficient charge-transfer pathways, and pronounced charge recombination at the dye/$TiO_2$/electrolyte interface, all of which suppress device efficiency [4–6].

Ultimately, DSSC performance hinges on a delicate balance: the light-harvesting capability of the sensitizer and the efficiency with which charges transfer across the interfaces. This directly explains why reported photovoltaic efficiencies for DSSCs vary widely with the botanical origin and exact chemical composition of the extracted pigments. For instance, while sensitizers from *Beta vulgaris* [7], *Rhus coriaria* [8], and *Prunus cerasus* [9] have broken the 1% PCE threshold, a vast majority of other plant extracts yield far more modest results. In our previous work with *Hyoscyamus reticulatus* extracts [10], we noted that efficient charge separation and suppression of recombination losses are important factors in determining the device's efficiency. This is in close agreement with prior literature, which highlights that recombination kinetics are fundamental to determining DSSC performance [11].

While the literature documents in detail the light-harvesting traits of natural sensitizers and their final PCEs, the relationship between interfacial electrochemical processes and photovoltaic performance across structurally diverse plant dyes remains insufficiently understood. Bridging this gap demands a concerted effort that integrates spectroscopic and electrochemical analyses to untangle exactly how molecular architecture dictates electron transport, recombination pathways, and system-level device operation.

Here, we comparatively investigate the potential of natural dyes extracted from *GG*, *CO*, and *CR* to serve as a highly reproducible and low-cost platform for natural dye-sensitized DSSCs (n-DSSCs). Characterization techniques such as Fourier-transform infrared (FT-IR), UV–Vis, and electrochemical impedance spectroscopy (EIS), as well as current density–voltage ($J$–$V$) analysis, were used to determine the structural, optical, and electrochemical properties of the dyes for DSSC devices. The main aim of the present work is to demonstrate the relationships among key factors that determine the photovoltaic performance of the DSSC device, including light-harvesting efficiency, interfacial charge-transfer kinetics, and charge-recombination dynamics.

## 2. Experimental

### 2.1. Plant materials

Three plant-derived natural dyes were used as sensitizers in this study: *Glaucium grandiflorum* Boiss. & A.Huet, *Consolida orientalis* (J.Gay) Schrödinger, and *Campsis radicans* (L.) Seem. Figure 1 shows the natural dye sources.

*Consolida orientalis* (J.Gay.) Schrödinger

*Consolida* (DC.) S.F. Gray (figure 1), a genus in the family Ranunculaceae, is distributed from the Western Mediterranean to Central Asia, and Anatolia is considered the center of diversity for this genus [12]. The chemical constituents of *Consolida* have been investigated since the beginning of the 20th century. Many members of the genus contain important phytochemicals, including diterpenoid alkaloids, flavonoids, phenolic acids, phytosterols, fatty acids, and volatile compounds [13]. *Consolida orientalis*, known as 'morçiçek' in Türkiye [14], is recognized by its 20–74 cm, simple or sparingly branched stems, laciniae, linear-setaceous leaves, intense violet flowers, and follicle fruit [12]. In this study, the violet flowers of the species were used.

*Glaucium grandiflorum* Boiss. & A.Huet

*Glaucium* Mill. (figure 1) A genus belonging to the Papaveraceae family is mainly distributed from Atlantic Europe to Central Asia [15]. *Glaucium* has been used in traditional medicine as a laxative, hypnotic, and antidiabetic agent. Leaves of *Glaucium* species are also used to treat dermatitis [16]. Numerous alkaloids have been isolated from *Glaucium* species. Although the identified alkaloid classes include aporphines, benzylisoquinolines, protopines, benzopheneanthridines, morphinanes, and




**Figure 1.** Photographic images of the natural dye sources used in this study: *Glaucium grandiflorum, Consolida orientalis*, and *Campsis radicans*.

protoberberinenes, aporphines are the dominant alkaloids in the genus [17]. The petals of *Glaucium grandiflorum* were used in this study.

*Campsis radicans* (L.) Seem.
*Campsis radicans* (figure 1), belonging to the family Bignoniaceae, is a climbing, woody plant distributed across the USA, Canada, China, and South Asia [18]. It is often grown as an ornamental plant in parks and gardens. It is used in traditional medicine for wound healing, treatment of infections caused by *Candida* and *Haemophilus*, and as an anti-itching medication [19]. In this study, the orange petals of the species were used.

### 2.2. DSSC fabrication and characterization

Fresh flower petals of *GG*, *CO*, and *CR* were washed with deionized water and dried under ambient conditions before extraction. The dyes were extracted in ethanol under continuous magnetic stirring at room temperature for 24 h. The resulting solutions were filtered to remove insoluble residues and used directly without further purification.

Fluorine-doped tin oxide (FTO) glass substrates were employed as transparent conductive electrodes. Prior to $TiO_2$ deposition, the substrates were sequentially cleaned by ultrasonication in acetone, ethanol, and deionized water. A compact $TiO_2$ blocking layer was subsequently formed by spin-coating a 40 mM aqueous $TiCl_3$ solution onto the FTO substrates, followed by thermal treatment at 70 °C for 30 min.

The mesoporous $TiO_2$ layer was prepared using a paste composed of P25 $TiO_2$ nanoparticles, ethyl cellulose, terpineol, and ethanol, with weight ratios of 13.2:46.8:4:36, respectively [20]. The mixture was homogenized using a high-speed mixer operating at 3500 rpm for 5 min. The prepared paste was deposited onto the substrates by spin coating at 4000 rpm for 5 min, then annealed at 500 °C for 1 h to remove organic components. A $TiCl_4$ post-treatment was then applied at 450 °C for 30 min to improve interparticle connectivity and surface activity.

The prepared photoanodes were immersed in *GG*, *CO*, and *CR* dye solutions at room temperature for 18 h to achieve sensitization, then rinsed with deionized water. Platinum-coated counter electrodes were prepared using a Pt precursor solution [21]. The DSSCs were assembled by sandwiching the liquid electrolyte (EL7) between the dye-sensitized photoanode and the counter electrode. The detailed composition of the EL7 electrolyte is reported elsewhere [22]. The fabrication procedure and operating mechanism of the fabricated DSSCs are schematically illustrated in figure 2.

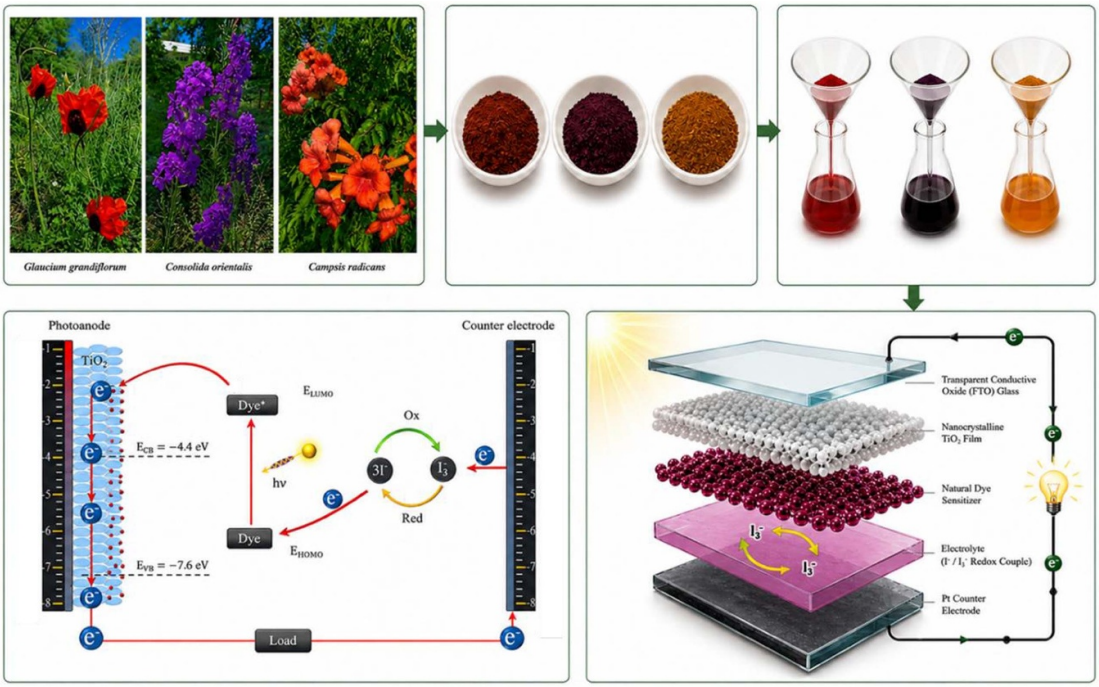



**Figure 2.** Schematic illustration of natural dye extraction, DSSC fabrication, and the photoinduced electron-transfer mechanism in DSSCs.

The functional groups of the extracted natural dyes were studied by FT-IR spectroscopy, particularly the hydroxyl and carbonyl groups, which are important for anchoring dye molecules on the $TiO_2$ surface and for efficient electron injection in DSSCs. Optical properties of dyes and bare and dye-loaded photoanodes were measured using a Shimadzu UV-1700 UV–vis spectrophotometer. Photovoltaic measurements were performed under AM 1.5G simulated solar illumination (100 mW $cm^{-2}$) using a solar simulator system. The *J–V* characteristics of the fabricated DSSCs were recorded to determine the photovoltaic parameters. In addition, *EIS* measurements were conducted to evaluate interfacial charge-transfer resistance and recombination behavior in the devices.

## 3. Results and discussion

### 3.1. Chemical composition of extracted dyes

Phytochemical investigations have validated that the dyes extracted from *GG*, *CO*, and *CR* contain a range of alkaloids, flavonoids, and phenolic compounds that may enhance visible-light absorption and interfacial interactions in DSSCs. The *GG*-derived dye is particularly abundant in isoquinoline alkaloids with protopine, aporphine, and benzylisoquinoline derivatives, including allocryptopine, isocorydine, reticuline, and N-methylcanadine [17]. Dye obtained from *CO* contains an array of alkaloids, including delcosine, gigactonine, takaosamine, and 18-dimethylpubescenine, in addition to phenolic acids and flavonoids (gallic acid, rosmarinic acid, quercetin, and kaempferol) [23, 24]. Research on the dye obtained from *CR* revealed the presence of phenolic and flavonoid compounds, as well as triterpenoid derivatives, including $\beta$-amyrin and arjunolic acid. [25].

Although the individual constituents of the extracts were not chromatographically separated in the present study, the literature-reported phytochemical profiles, together with the FT-IR and UV–Vis results, provide a reasonable basis for identifying the principal classes of photoactive chromophores. The sensitizing activity of these extracts is unlikely to arise from a single molecular species; rather, it is attributable to the combined contributions of several conjugated constituents. Flavonoids and related phenolic compounds contain aromatic $\pi$-systems, conjugated carbonyl groups, and hydroxyl substituents that act as auxochromes, promoting electron delocalization and shifting absorption toward the visible region. In *CO*, quercetin- and kaempferol-type flavonoids, together with other phenolic constituents, are therefore considered among the probable contributors to the observed optical response. The *GG* extract contains structurally diverse isoquinoline alkaloids and phenolic constituents; however, not all these

compounds necessarily function as effective visible-light chromophores, and the measured absorption most likely reflects the collective response of the conjugated components present in the crude extract. Similarly, the comparatively strong and broad visible-light absorption of *CR* suggests a greater abundance and/or broader distribution of conjugated flavonoid-, phenolic-, and pigment-type constituents. The O–H and C=O bands detected by FT-IR further support the presence of oxygen-containing chromophoric structures and functional groups that interact with surface Ti sites. Accordingly, the natural dyes examined here should be regarded as multicomponent sensitizer systems in which several photoactive constituents contribute cooperatively to light harvesting and semiconductor adsorption. Nevertheless, because no chromatographic separation or mass spectrometric identification was performed, the assignment of the absorption bands to specific molecular chromophores remains tentative. Future HPLC-DAD and LC-MS/MS analyses will be required to identify and quantify the principal photoactive compounds and to establish their individual contributions to the photovoltaic response.

The extended π-conjugated frameworks and hydroxyl/carbonyl functionalities present in these compounds may promote efficient electronic communication with $TiO_2$, thereby facilitating sensitization in DSSCs. Such structural characteristics enhance both visible-light harvesting and dye adsorption onto the semiconductor surface. Furthermore, phenolic and flavonoid constituents, together with alkaloids, provide chemically versatile photoactive architectures that can support interfacial electron injection and charge-transfer processes.

### 3.2. Spectroscopic analysis and optical properties of natural dyes and photoanodes

Figure 3 presents the FT-IR spectra of *GG*, *CO*, and *CR* dye extracts (figure 3(a)), the UV–Vis absorption spectra of the dye solutions (figure 3(b)), and the UV–Vis spectra of bare and dye-sensitized $TiO_2$ photoanodes (figure 3(c)). These analyses provide insight into the functional groups responsible for dye adsorption as well as the optical behavior of the sensitizers. The FT-IR spectra of all dye extracts reveal characteristic hydroxyl (O–H) and carbonyl (C=O) vibrational bands, indicating the presence of oxygen-containing functional groups that can enhance dye adsorption onto $TiO_2$ surfaces and facilitate electron injection upon photoexcitation [26].

The carbonyl stretching bands in *CR* and *CO* dye extracts are at the same positions, 1731 and 1729 $cm^{-1}$, respectively, indicating a similar chemical environment for the carbonyl-containing species. In contrast, a carbonyl stretching band of *GG* dye extract is observed at a lower wavenumber (1700 $cm^{-1}$), which might be due to increased conjugation effects or intermolecular interaction inside the extract composition. The O–H stretching bands observed for *CR* and *CO* dye extracts at around 3335 and 3336 $cm^{-1}$ indicated the presence of hydrogen-bonded hydroxyl groups. *GG* dye extract exhibited a sharper O–H band centered at 3615 $cm^{-1}$, which corresponds largely to non-hydrogen-bonded hydroxyl species. These differences indicate that the intermolecular interactions and possibly the adsorption behavior of the studied dyes differ. In general, the FT-IR results show that all the extracts contain functional groups that can interact with $TiO_2$ surfaces, which is important for sensitization and interfacial electron transfer processes in DSSCs.

The UV–Vis absorption spectra of the dye solutions are shown in figure 3(b). All the natural dye extracts exhibit absorption in the visible region, confirming their potential as sensitizers in DSSCs. The broad absorption characteristics observed in the natural dye extracts suggest the presence of various chromophoric constituents, such as flavonoids and phenolic compounds, which account for the broadened spectral response. The enhancement of absorption in the visible-light region for the *CR* natural dye can be explained by the higher concentration of optically active compounds and more efficient adsorption on the $TiO_2$ surface. For efficient photoinduced electron injection, not only improved optical absorption and interactions between dye molecules and the $TiO_2$ surface are necessary. Figure 3(c) shows the UV–Vis spectra of bare and dye-sensitized $TiO_2$ photoanodes. All the dye-sensitized photoanodes exhibit significantly higher absorption in the 400–700 nm range than the bare $TiO_2$ photoanode, indicating successful sensitization and improved visible-light harvesting. [27] Among the dyes studied, the highest absorbance over the visible region was observed for the *CR* natural dye-sensitized photoanode, followed by *CO* and *GG* natural dyes. The enhanced and extended absorption profiles of the dye-sensitized photoanodes are therefore expected to improve the photocurrent generation and the DSSC performance.

### 3.3. Photovoltaic performance

Figure 4 shows the *J–V* characteristics of the DSSCs sensitized with *GG*, *CO*, and *CR* natural dyes, while the extracted photovoltaic parameters are summarized in table 1. To evaluate the reproducibility and reliability of the fabricated DSSCs, five independent devices were fabricated and tested for each natural dye sensitizer under identical conditions. Each photovoltaic parameter is presented in table 1.

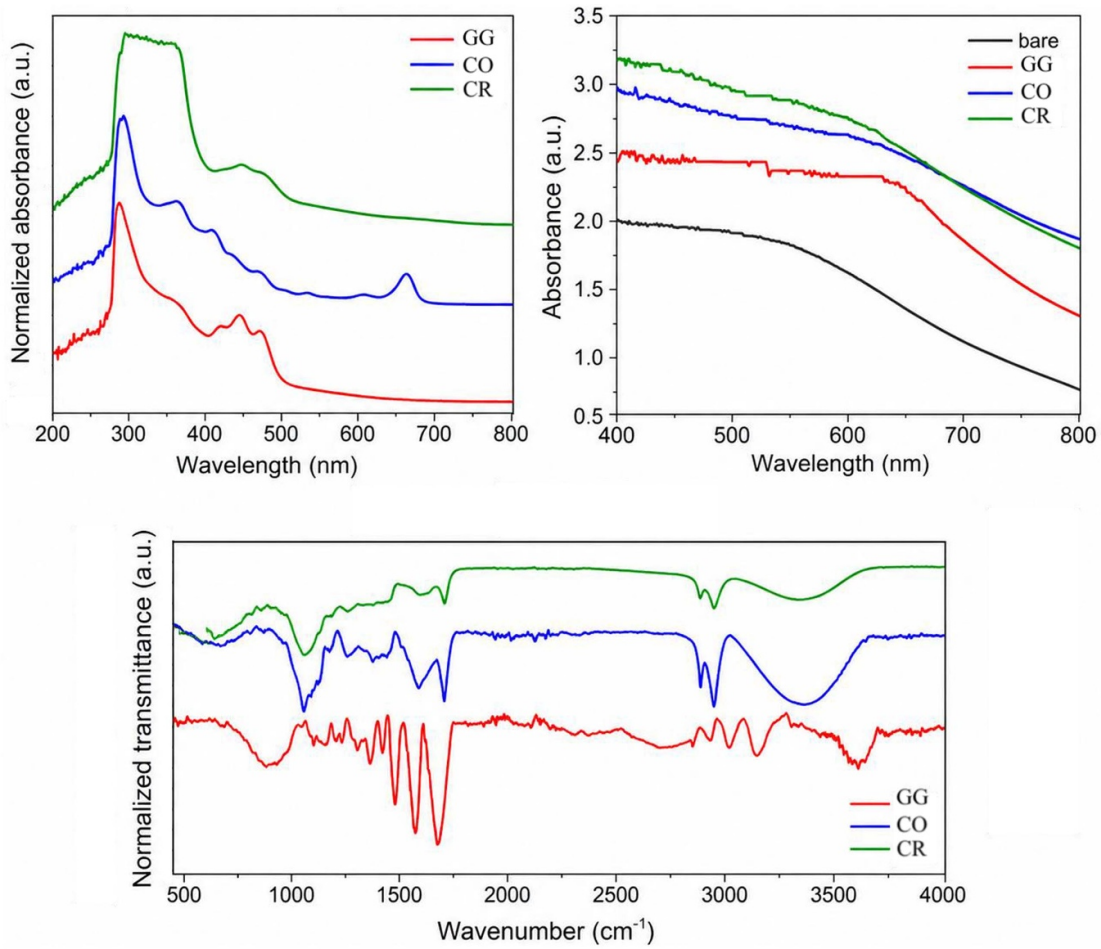



**Figure 3.** (a) FT-IR spectra of *GG*, *CO*, and *CR* dye extracts, (b) UV–Vis absorption spectra of the dye solutions, and (c) UV–Vis spectra of bare and dye-sensitized $TiO_2$ photoanodes.

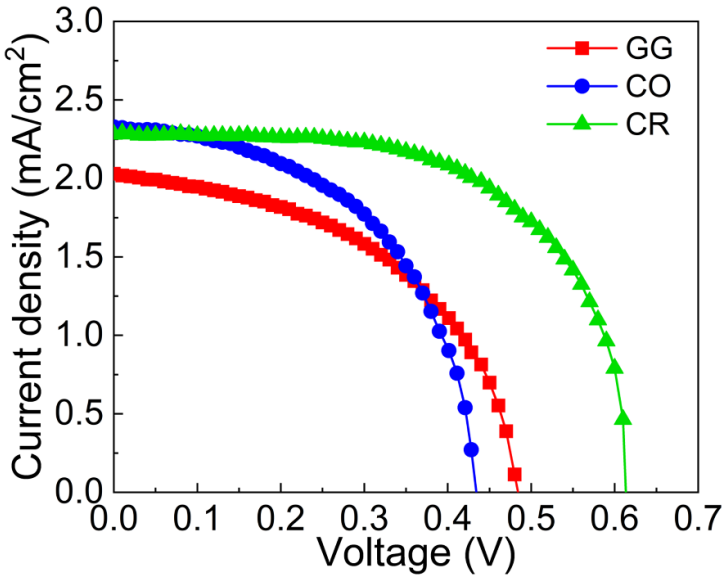



**Figure 4.** *J–V* curves of DSSCs sensitized with *GG*, *CO*, and *CR* natural dyes.

Primarily, the results show that all fabricated devices exhibited some efficiency, indicating that efficient electron injection and dye regeneration were successfully achieved among the dyes, $TiO_2$, and the electrolyte.

**Table 1.** Photovoltaic parameters of DSSCs sensitized with *GG*, *CO*, and *CR* under AM 1.5G illumination[a].

| Dyes | $J_{SC}$ (mA cm$^{-2}$) | $V_{OC}$ (V) | *FF* | *PCE* (%) | $R_{sh}(\Omega)$ | $R_{se}(\Omega)$ |
|---|---|---|---|---|---|---|
| *GG* | 2.03 ± 0.14 | 0.48 ± 0.01 | 0.49 ± 0.01 | 0.49 ± 0.03 | 4463.18 ± 228.05 | 159.76 ± 12.94 |
| *CO* | 2.33 ± 0.01 | 0.43 ± 0.01 | 0.52 ± 0.01 | 0.53 ± 0.01 | 5772.55 ± 222.48 | 167.83 ± 13.77 |
| *CR* | 2.28 ± 0.1 | 0.61 ± 0.01 | 0.55 ± 0.01 | 0.78 ± 0.01 | 14 474.8 ± 3392.99 | 130.78 ± 12.96 |

[a] Values are reported as mean ± standard deviation for five independently fabricated devices ($n = 5$).

As shown in the results, the *CR*-based DSSCs exhibited the most encouraging photovoltaic performance among the examined dyes, achieving a maximum PCE of 0.78%. This performance was accompanied by a short-circuit current density ($J_{SC}$) of 2.28 mA cm$^{-2}$, an open-circuit voltage ($V_{OC}$) of 0.61 V, and an fill factor (*FF*) of 0.55. Although the overall photovoltaic performance of *CR* is consistent with its stronger visible-light absorption observed in the UV–Vis analysis, it does not, contrary to general expectations, exhibit the highest $J_{SC}$ value. Specifically, the *CO*-based device exhibited the highest $J_{SC}$ (2.33 mA cm$^{-2}$) despite *CR*'s superior optical absorption, delivering a PCE of 0.53%, a $V_{OC}$ of 0.43 V, and an *FF* of 0.52. This discrepancy can be attributed to several interdependent factors, including potential differences in quantitative dye loading, actual surface coverage, light-harvesting capacity, as well as interfacial resistances and recombination losses. Consequently, although the *CO*-based device achieved the highest $J_{SC}$, its lower $V_{OC}$ limited the overall PCE. On the other hand, the *GG*-based DSSC showed the lowest photovoltaic performance, with a PCE of 0.49% and a reduced $J_{SC}$ value of 2.03 mA cm$^{-2}$. The lower photovoltaic performance of the *GG*-based DSSC likely stems from weaker light absorption and less favorable interfacial charge transfer. Since multiple variables influence the generated photocurrent, our investigation focused on interfacial charge-transfer kinetics to better understand the mechanisms governing the ultimate device efficiency. As the subsequent internal resistance and electrochemical impedance analyses indicate, the improved overall performance of the *CR*-sensitized device is closely associated with its ability to effectively suppress interfacial charge recombination. As one of the main outputs of this study, it was concluded that enhanced optical absorption alone is insufficient to achieve higher device efficiency without favorable interfacial charge-transfer characteristics. To provide a more detailed explanation of the fundamental physical mechanisms governing the charge transport properties, *FF*, and overall PCE of the cells. Accordingly, the series resistance ($R_{se}$) and shunt resistance ($R_{sh}$) parameters extracted from the *J–V* curves were evaluated. In a typical DSSC, while the $R_{se}$ derived from the *J–V* plot represents the total ohmic resistance along the forward charge-transmission pathway, the shunt resistance ($R_{sh}$) is a direct indicator of internal leakage currents and the tendency toward charge recombination. It is well known that a cell with low $R_{se}$ and high $R_{sh}$ values achieves a high *FF* [28, 29], thereby leading to a higher PCE.

The comparatively higher $V_{OC}$ and *FF* values obtained for the *CR*-based device suggest more efficient charge collection and reduced recombination losses within the DSSC structure, which is mechanistically supported by the device's macroscopic resistance parameters ($R_{se}$ and $R_{sh}$). As shown in table 1, the *CR* sample exhibits a drastically reduced $R_{se}$ of 130.78 Ω and a remarkably high $R_{sh}$ of 14 474.8 Ω. This massive increase in $R_{sh}$ improves the leakage characteristics of the *J–V* curve, minimizes current leakage, and prevents the drop in maximum deliverable power, thereby directly contributing to a higher *FF*. Simultaneously, the low $R_{se}$ reduces internal ohmic losses along the transmission pathway, facilitating superior forward charge transport. Therefore, the synergistic combination of this exceptionally high $R_{sh}$ and low $R_{se}$ is the primary physical mechanism responsible for the highest *FF* (0.55) achieved by the *CR*-sensitized device.

On the other hand, the *GG* and *CO* samples exhibit relatively higher series resistances (159.76 Ω and 167.83 Ω, respectively) and dramatically lower shunt resistances (4463.18 Ω and 5772.55 Ω, respectively) when compared to the *CR* device. The significantly lower $R_{sh}$ values in *GG* and *CO* indicate a pronounced tendency toward dark-current leakage and recombination within the cells. These leakages deplete the electron density within the $TiO_2$ film and lower the Fermi level, leading to the reduced $V_{OC}$ values observed. Ultimately, the comprehensive analysis of photovoltaic and internal resistance ($R_{se}$ and $R_{sh}$) results indicates that *CR* offers a more balanced combination of light-harvesting and interfacial charge-transfer behavior among the investigated natural sensitizers. The effects of interfacial charge-transfer dynamics on DSSC performance are examined in more detail in the next section using EIS measurements.

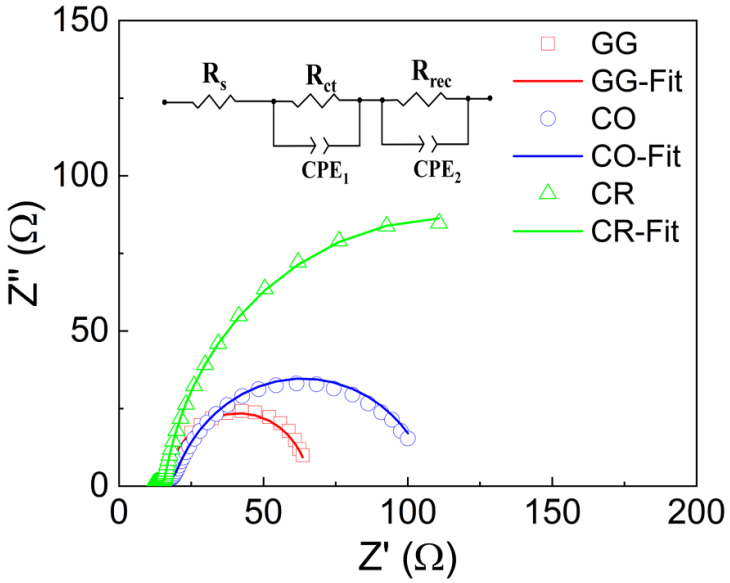



**Figure 5.** Experimental and fitted EIS Nyquist plots of the fabricated DSSCs, together with the equivalent circuit model.

**Table 2.** EIS parameters of DSSCs sensitized with *GG*, *CO*, and *CR* using EL7 electrolyte.

| Dyes | $R_s$ (Ω) | $R_{ct}$ (Ω) | $R_{rec}$ (Ω) | $\eta_{cc}$ (%) | $\chi^2$ |
|---|---|---|---|---|---|
| *GG* | 14.33 | 4.61 | 47.27 | 91.11 | 0.000 716 |
| *CO* | 14.29 | 4.52 | 89.74 | 95.20 | 0.000 218 |
| *CR* | 11.48 | 4.34 | 197.30 | 97.84 | 0.000 124 |

### 3.4. EIS

To study the charge-transfer and recombination processes in *GG*-, *CO*-, and *CR*-sensitized DSSCs, we performed EIS measurements. Figure 5 displays the Nyquist plots of the devices and the equivalent electrical circuit for fitting. The parameters extracted from EIS are presented in table 2. In the applied equivalent circuit, constant phase elements (CPE1 and CPE2) are used instead of ideal capacitors to represent non-ideal capacitive behavior arising from the porous nature and surface roughness of the interfaces. Specifically, CPE1 (dominant in the high-frequency region) is connected in parallel with the charge-transfer resistance ($R_{ct}$) to accurately model the non-ideal double-layer capacitance at the counter electrode/electrolyte interface. On the other hand, CPE2 (operating in the mid-frequency region) is connected in parallel with the recombination resistance ($R_{rec}$). CPE2 reflects the chemical capacitance, representing the photoexcited electron storage capacity and surface heterogeneity at the $TiO_2$/dye/electrolyte interface. The application of these phase elements provides a highly accurate representation of interfacial heterogeneity, which directly influences charge transfer and recombination kinetics [30, 31].

The accuracy of the applied equivalent circuit model was mathematically verified by the low goodness-of-fit ($\chi^2$) values extracted from the software, which are incorporated in table 2. The good agreement between experimental data and fitted curves also confirms the reliability of the calculated parameters for interfacial charge transfer and recombination resistance. In the EIS equivalent circuit model, $R_s$ is the series resistance of the FTO substrate, $R_{ct}$ is the charge-transfer resistance at the counter electrode/electrolyte interface, and $R_{rec}$ is the electron recombination at the $TiO_2$/dye/electrolyte interface. The photovoltaic performance differences were primarily attributable to variations in interfacial electrochemical parameters, particularly $R_{ct}$ and $R_{rec}$, since all DSSCs were fabricated on the same FTO substrates. In DSSCs, lower $R_{ct}$ values are associated with more efficient charge-transfer processes, while higher $R_{rec}$ values are associated with suppressed electron recombination and reduced interfacial charge losses [32, 33]. In our case, the *CR*-based DSSC exhibited the lowest $R_{ct}$ and the highest $R_{rec}$ values, indicating more favorable charge-transfer behavior together with more effective suppression of recombination processes. In contrast, the *GG*-based device exhibited lower recombination resistance, indicating increased charge losses within the cell. The *CO*-based DSSC exhibited electrochemical characteristics intermediate between *GG* and *CR*. These results are consistent with the photovoltaic measurements, which showed that the *CR* sensitizer achieved the highest *PCE*.

**Table 3.** Comparison of photovoltaic parameters of n-DSSCs reported in the literature and this work.

| Source | $J_{SC}$ (mA cm$^{-2}$) | $V_{OC}$ (V) | *FF* | *PCE* (%) | References |
|---|---|---|---|---|---|
| *Hedera helix* L. | 2.35 | 0.65 | 0.77 | 1.17 | [2] |
| *Punica granatum* L. | 0.97 | 0.59 | 0.85 | 0.49 | [3] |
| *Linaria grandiflora* Desf. | 0.70 | 0.52 | 0.67 | 0.24 | [3] |
| *Cota tinctoria* (L.) J. Gay | 2.11 | 0.57 | 0.76 | 0.91 | [3] |
| *Beta vulgaris (rubra)* | 9.5 | 0.42 | 0.37 | 1.70 | [7] |
| *Rhus coriaria* L. | 9.3 | 0.39 | 0.41 | 1.50 | [8] |
| *Prunus cerasus* L. | 3.90 | 0.58 | 0.56 | 1.27 | [9] |
| *Hyoscyamus reticulatus* L. | 2.66 | 0.67 | 0.67 | 1.20 | [11] |
| *Mahonia aquifolium* (Pursh) Nutt. | 1.34 | 0.45 | 0.37 | 0.22 | [11] |
| *Melastoma malabathricum* L. | 6.17 | 0.383 | 0.44 | 1.16 | [35] |
| *Hibiscus surattensis* L. | 5.45 | 0.39 | 0.54 | 1.14 | [36] |
| *Parthenocissus quinquefolia* L. | 2.08 | 0.54 | 0.63 | 0.72 | [37] |
| *Ligustrum vulgare* L. | 0.85 | 0.64 | 0.88 | 0.48 | [38] |
| *Juniperus sabina* L. | 1.02 | 0.66 | 0.82 | 0.55 | [38] |
| *Papaver rhoeas* L. | 1.22 | 0.56 | 0.62 | 0.42 | [38] |

In addition, the charge-collection efficiency ($\eta_{cc}$) was determined by the relation $\eta_{cc} = [1 + (R_{ct}/R_{rec})]^{-1}$ [34]. The higher $\eta_{cc}$ value indicates more efficient electron collection and lower recombination losses in the DSSC structure. In agreement with the EIS analysis, the CR-based device exhibited the highest $\eta_{cc}$ value, further confirming its improved interfacial charge-transfer properties.

The results from the EIS and *J–V* characterization for the fabricated DSSCs are in good agreement with the optical analyses when considered together. These results demonstrate the significance of interfacial charge-transfer kinetics on the overall device performance. The photocurrent for the *CO* extract is comparatively higher, while the EIS results show higher recombination resistance ($R_{rec}$) at the electrode-electrolyte interface in the *CR*-sensitized cell. The higher $R_{rec}$ value indicates that the *CR* dye can reduce back-electron transfer from $TiO_2$ to the electrolyte. Consequently, the higher $V_{OC}$, *FF*, and overall PCE observed for the *CR* cell appear to be closely related to these favorable interfacial charge-transfer dynamics, alongside its optical properties.

### 3.5. Comparison with previously reported n-DSSCs

To further evaluate the performance of the investigated sensitizers, the photovoltaic parameters obtained in this study were compared with those reported for previously reported n-DSSCs, as summarized in table 3. Reported efficiencies of natural sensitizers vary considerably depending on dye composition, extraction conditions, adsorption behavior, and interfacial charge-transfer characteristics.

Among the investigated sensitizers, the *CR*-based DSSCs achieved a moderate PCE of 0.78%, which is comparable to several previously reported plant-derived dyes. In particular, the relatively high $V_{OC}$ and enhanced recombination resistance of the *CR*-based device distinguish it from many natural dye systems, in which performance is primarily associated with increased photocurrent generation.

Previous studies, including our earlier investigations of *Punica granatum, Cota tinctoria, Hedera helix*, and *Hyoscyamus reticulatus*, have shown that DSSC efficiency is strongly influenced not only by visible-light absorption but also by interfacial charge transfer and recombination dynamics. The present results further support this interpretation. Although some natural sensitizers reported in the literature exhibit higher photocurrent densities and efficiencies, the *EIS* analysis demonstrates that the *CR* sensitizer provides comparatively efficient suppression of charge recombination together with favorable charge-collection behavior.

Overall, the comparative analysis indicates that achieving efficient interfacial charge-transfer regulation is as important as broad optical absorption for improving n-DSSCs. The combined optical, photovoltaic, and electrochemical results suggest that natural dye extracted from *CR* is a promising natural sensitizer due to its balanced light-harvesting and recombination-suppression characteristics.

## 4. Conclusion

In this study, natural dyes extracted from *GG*, *CO*, and *CR* were comparatively investigated as sensitizers for DSSCs. The combined spectroscopic, photovoltaic, and electrochemical analyses demonstrated that DSSC performance is strongly influenced not only by visible-light absorption but also by interfacial

charge-transfer and recombination processes. Among the investigated dyes, the *CR*-based DSSC exhibited the highest photovoltaic performance, achieving a PCE of 0.78% together with improved $V_{OC}$ and charge-collection efficiency. *EIS* analysis further revealed that the enhanced performance of *CR* is associated with higher recombination resistance and reduced interfacial charge losses. The obtained results indicate that, for the investigated natural extracts, effective control of interfacial recombination, together with optical absorption, plays an important role in determining device performance. Although achieving a record-high efficiency was not the primary objective of this study, the results provide valuable mechanistic insights into the photovoltaic behavior of natural sensitizers. While the efficiencies remain lower than those of state-of-the-art synthetic dyes, the low-cost production, simple extraction procedures, and environmentally friendly nature of natural dyes offer considerable potential for sustainable photovoltaic applications. In particular, the 0.78% PCE achieved by *CR* is competitive within the class of plant-derived n-DSSCs, highlighting its potential as a low-cost, non-toxic sensitizer. Nevertheless, long-term stability and photodegradation remain important challenges for natural-dye-based devices and should be addressed in future studies before their practical application can be fully assessed.

## Acknowledgment

This work was supported by the Kırşehir Ahi Evran University Scientific Research Projects Coordination Unit. (Project Number: ZRT.A2.24.001).

## Data availability statement

The data that support the findings of this study are available upon reasonable request from the authors. The research data have not been deposited in a public repository. However, all data supporting the findings of this study are available from the corresponding author upon reasonable request.

## Author contributions

M Erdoğdu 0000-0001-8255-2041
Conceptualization (equal), Data curation (equal), Investigation (equal), Methodology (equal), Project administration (equal), Writing – original draft (equal)

K Ozel 0000-0002-0250-3731
Conceptualization (equal), Data curation (equal), Investigation (equal), Methodology (equal), Writing – original draft (equal)

M E Yelkovan 0009-0006-9066-0724
Conceptualization (equal), Data curation (equal), Investigation (equal), Methodology (equal)

A Yildiz 0000-0003-4137-6971
Investigation (equal), Methodology (equal), Writing – original draft (equal), Writing – review & editing (equal)

B Altun 0000-0002-6503-7109
Conceptualization (equal), Data curation (equal), Investigation (equal), Methodology (equal)

Y Erdogdu 0000-0001-7695-3834
Investigation (equal), Methodology (equal), Resources (equal), Writing – original draft (equal), Writing – review & editing (equal)

## References

[1] O'regan B and Grätzel M 1991 A low-cost, high-efficiency solar cell based on dye-sensitized colloidal $TiO_2$ films *Nature* **353** 737–40

[2] Erdogdu M, Atilgan A, Erdogdu Y and Yildiz A 2024 Flavonoid from *Hedera helix* fruits: a promising new natural sensitizer for DSSCs *J. Photochem. Photobiol. A* **448** 115288

[3] Yelkovan M E, Erdogdu M, Özbek M U, Erdogdu Y and Yildiz A 2026 Mechanistic correlation between electron injection, recombination, and photovoltage in *Cota tinctoria, Punica granatum*, and *Linaria grandiflora*-based natural dye-sensitized solar cells *Mater. Res. Express* **13** 025502

[4] Teja A S, Srivastava A, Satrughna J A K, Tiwari M K, Kanwade A, Yadav S C and Shirage P M 2022 Optimal processing methodology for futuristic natural dye-sensitized solar cells and novel applications *Dyes Pigm.* **210** 110997

[5] Iman R N, Harrabi K, Younas M and Mekki A 2024 Fabrication of efficient natural dye-sensitized solar cells using Mediterranean olive leaves as natural dye sensitizer *J. Photochem. Photobiol. A* **450** 115477

[6] Golshan G, Osfouri S, Azin R, Jalali T and Moheimani N R 2021 Co-sensitization of natural and low-cost dyes for efficient panchromatic light-harvesting using dye-sensitized solar cells *J. Photochem. Photobiol. A* **417** 113345

[7] Calogero G, Di Marco G, Cazzanti S, Caramori S, Argazzi R, Di Carlo A and Bignozzi C A 2010 Efficient dye-sensitized solar cells using red turnip and purple wild Sicilian prickly pear fruits *Int. J. Mol. Sci.* **11** 254–67

[8] Ali Al-bat'hi S, Alaei I and Sopyan I 2013 Natural photosensitizers for dye sensitized solar cells *Int. J. Renew. Energy Res.* **3** 138–43

[9] Steephen A, Saini K, Suvitha A, Vivek P, Arumanayagam T, Rekha M and Madhavan B 2023 Investigational and computational explorations on betanin, lycopene, cyanidin, and peonidin organic photosensitizers for green energy harvesting *Sustain. Energy Technol. Assess.* **60** 103451

[10] Yelkovan M E, Erdogdu M, Erdogdu Y and Yildiz A 2025 Driving forces of injection and regeneration in natural dye-sensitized solar cells: insights into photovoltaic performance *Sol. Energy* **295** 113523

[11] Tractz G T, Viomar A, Dias B V, de Lima C A, Banczek E P, da Cunha M T, Antunes S R M and Rodrigues P R P 2019 Recombination study of dye sensitized solar cells with natural extracts *J. Braz. Chem. Soc.* **30** 371–8

[12] Davis P H 1965 *Flora of Turkey and the East Aegean Islands* vol 1 (Edinburgh University Press)

[13] Yin T, Cai L and Ding Z 2020 A systematic review on the chemical constituents of the genus *Consolida* (Ranunculaceae) and their biological activities *RSC Adv.* **10** 35072–89

[14] Güner A, Aslan S, Ekim T, Vural M and Babaç M T 2012 *Türkiye Bitkileri Listesi (Damarlı Bitkiler)* (Nezahat Gökyiğit Bahçesi ve Flora Araştırmaları Derneği Yayını)

[15] Kadereit J W 1993 *Glaucium. In the Families and Genera of Vascular Plants* ed K Kubitzki, J C Rohwer and V Bittrich (Springer) pp 1–663

[16] Morteza-Semnani K, Saeedi M, Hamidian M, Vafamehr H and Dehpour A R 2002 Anti-inflammatory, analgesic activity and acute toxicity of *Glaucium grandiflorum* extract *J. Ethnopharmacol.* **80** 181–6

[17] Akaberi T, Shourgashti K, Emami S A and Akaberi M 2021 Phytochemistry and pharmacology of alkaloids from *Glaucium* spp *Phytochemistry* **191** 112923

[18] Wen J and Jansen R K 1995 Morphological and molecular comparisons of *Campsis grandiflora* and *C. radicans* (Bignoniaceae), an eastern Asian and eastern North American vicariad species pair *Plant Syst. Evol.* **196** 173–83

[19] Michael M 1989 *Medicinal Plants of the Desert and Canyon West* (Museum of New Mexico Press) p 124

[20] Ozel K, Atilgan A and Yildiz A 2024 Multi-layered blocking layers for dye sensitized solar cells *J. Photochem. Photobiol. A* **448** 115297

[21] Ozel K, Kosalay I, Atilgan A, Atli A, Yildiz Z K and Yildiz A 2018 Performance improvement of dye-sensitized solar cells with AZO and BZO blocking layers *J. New Mater. Electrochem. Syst.* **21** 227–31

[22] Bifari E N, Nhari L M, El-Shishtawy R M, Asiri A M, Ozel K, Atilgan A and Yildiz A 2025 Phenothiazine-imidazole-based dye containing furan $\pi$-linker for dye-sensitized solar cells *J. Mater. Sci.* **61** 905–17

[23] Hohmann J, Forgo P, Hajdú Z, Varga E and Máthé I 2002 Norditerpenoid alkaloids from *Consolida orientalis* and complete $^{1}$H and $^{13}$C NMR signal assignments of some lycoctonine-type alkaloids *J. Nat. Prod.* **65** 1069–72

[24] Gürer E S, Karadağ A E, Baydar R and Demirel M 2024 Investigation of the chemical composition, antioxidant and anti-cholinesterase activities of *Consolida orientalis J. Health Sci. Med.* **7** 691–5

[25] Karaduman T and Soylukan C 2024 *Bioactive Compounds from Campsis Radicans L.: Antioxidant and Antiproliferative Effects on Colon Cancer Cells* (Preprints. doi.org) (https://doi.org/10.20944/preprints202402.0930.v1)

[26] Erdogdu Y, Baskose U C, Saglam S, Erdogdu M, Ogutcu H and Özçelik S 2020 Structural, thermal, spectroscopic, electronic and biological activity properties of coumarin-153 dyes for DSSCs: a DFT benchmark study *J. Mol. Struct.* **1221** 128873

[27] Shi D 2025 Three-dimensional solar harvesting with transparent spectral selective photovoltaics in agrivoltaics *Energies* **18** 1788

[28] Yadav V, Chaudhary S, Negi C M S and Gupta S K 2020 Textile dyes as photo-sensitizer in dye-sensitized solar cells *Opt. Mater.* **109** 110306

[29] Kharkwal D, Sharma N, Gupta S K and Negi C M S 2021 Enhanced performance of dye-sensitized solar cells by co-sensitization of metal-complex and organic dye *Sol. Energy* **230** 1133–40

[30] Gupta S K and Negi C M S 2025 Photovoltaic performance evaluation of dye-sensitized solar cells made using a quasi-solid-state electrolyte and a low-cost pencil graphite counter electrode *Ionics* **31** 2045–55

[31] Yadav V, Negi C M S, Kumar D K and Gupta S K 2021 Fabrication of eco-friendly, low-cost dye-sensitized solar cells using harda fruit-based natural dye *Opt. Mater.* **122** 111800

[32] Mahalingam S, Manap A, Lau K S, Rabeya R, Chia C H, Xue K and Chelvanathan P 2025 Recombination suppression in $TiO_2$/boron-doped reduced graphene oxide-based dye-sensitized solar cells *Renew. Sustain. Energy Rev.* **209** 115088

[33] Li G, Liang M, Wang H, Sun Z, Wang L, Wang Z and Xue S 2013 Significant enhancement of open-circuit voltage in indoline-based dye-sensitized solar cells via retarding charge recombination *Chem. Mater.* **25** 1713–22

[34] Subramaniam M R, Kumaresan D, Jothi S, McGettrick J D and Watson T M 2018 Reduced graphene oxide wrapped hierarchical $TiO_2$ nanorod composites for improved charge collection efficiency and carrier lifetime in dye sensitized solar cells *Appl. Surf. Sci.* **428** 439–47

[35] Yusoff A, Kumara N T R N, Lim A, Ekanayake P and Tennakoon K U 2014 Impacts of temperature on the stability of tropical plant pigments as sensitizers for dye sensitized solar cells *J. Biophys.* **2014** 739514

[36] Wongcharee K, Meeyoo V and Chavadej S 2007 Dye-sensitized solar cell using natural dyes extracted from rosella and blue pea flowers *Sol. Energy Mater. Sol. Cells* **91** 566–71

[37] Akkuş A, Ozel K, Erdogdu M, Atılgan A, Yildiz A and Erdogdu Y 2026 Electrolyte-dependent photovoltaic performance of *Parthenocissus quinquefolia* natural dye in dye-sensitized solar cells *Mater. Lett.* **389** 140821

[38] Erdogdu M, Atilgan A, Erdogdu Y and Yildiz A 2024 Natural dyes extracted from *Ligustrum vulgare, Juniperus sabina*, and *Papaver rhoeas* for novel DSSC applications *Mater. Lett.* **358** 135811